

Sensorless position control of permanent magnet motors with pulsating current injection and compensation of motor end-effects

*Original*

Sensorless position control of permanent magnet motors with pulsating current injection and compensation of motor end-effects / Cupertino, F; Pellegrino, GIAN - MARIO LUIGI; Giangrande, P; Salvatore, L.. - In: IEEE TRANSACTIONS ON INDUSTRY APPLICATIONS. - ISSN 0093-9994. - STAMPA. - (2011). [10.1109/TIA.2011.2126542]

*Availability:*

This version is available at: 11583/2351344 since:

*Publisher:*

IEEE

*Published*

DOI:10.1109/TIA.2011.2126542

*Terms of use:*

This article is made available under terms and conditions as specified in the corresponding bibliographic description in the repository

*Publisher copyright*

(Article begins on next page)

# Sensorless position control of permanent magnet motors with pulsating current injection and compensation of motor end-effects

Francesco Cupertino, Member, IEEE, Gianmario Pellegrino, Member, IEEE,  
Paolo Giangrande, Student Member, IEEE, and Luigi Salvatore

**Abstract** -- The sensorless position control of permanent magnet motors is successfully implemented superimposing a high-frequency voltage signal on the voltage reference or adding a high-frequency current signal to the current reference. The former approach is usually preferred because of its simplicity although the latter one may allow better performance. This paper presents a new algorithm for sensorless control of low-saliency permanent magnet synchronous motors based on high-frequency sinusoidal current signal injection into the d-axis. Differently from the related literature, the position information is derived by analyzing the measured high-frequency currents. The amplitude of the d-axis voltage reference is also exploited to improve performance. A proportional integral controller plus resonant term is adopted to ensure accurate tracking of both the dc and high-frequency components of the d-axis current reference. The main advantages of the proposed approach are the increased accuracy and sensitivity with respect to the approach based on voltage injection, the insensitiveness to inverter non-linearities that are compensated by the current regulation loop, the actual control on the injected current value, and practical absence of acoustic noise. Experiments on a linear tubular permanent magnet synchronous motor prototype have been carried out to verify the above mentioned advantages. The paper also presents a discussion of the parameters of proportional integral controller plus resonant term.

**Index Terms** – End effects, high frequency signal injection, linear tubular permanent magnet motors, sensorless position control.

## I. INTRODUCTION

Linear permanent magnet motors are becoming increasingly widespread in automation applications because they permit to eliminate mechanical transmission devices. Among the commonly used structures for linear permanent magnet synchronous motors the tubular one allows to better exploit the permanent magnet flux reducing size and end effects. Similarly to rotating machines, the tubular permanent magnet synchronous motor (LTPMSM) need position information to synchronize the current vector to the permanent magnets position. Since low and zero speed operations are generally essential in practical application of such devices, signal injection-based schemes appear a necessary solution for sensorless operation. As a matter of fact, at low and zero speed the back EMF voltage magnitude is very small or zero. This makes all the techniques based on the back EMF unsuccessful [1]. Recently, a large effort has been dedicated to investigate techniques for position estimation of synchronous motors having low-saliency using the injection of high-frequency signals [2-4]. A high-frequency voltage (or current [5-6]) signal can be

superimposed on the motor reference voltages (or currents) to estimate the rotor position from the high-frequency components of the phase currents that are affected by the magnetic spatial motor saliency. This allows realizing sensorless schemes that don't require additional hardware, have low sensitivity to parameter variations and have been proven to be successful at low and zero speed. A comparison among the different approaches that can be used to realize a sensorless scheme via high-frequency signal injection can be found in [7-9].

In this paper we consider the approach based on the superimposition of a pulsating current vector (PCV) along the estimated d-axis at a constant frequency. Differently from [5-6] the proposed approach is based on the analysis of the measured d- and q-axis currents and the d-axis voltage reference at injection frequency. This approach is less sensitive to the inverter non-idealities because the d-axis control loop ensures a sinusoidal injected current and is almost acoustically noiseless also because the amount of electromagnetic torque generated by the injected high-frequency current signal is negligible. The proposed approach is based on a proper current controller that is a proportional integral controller plus resonant term (PI-RES). The tuning of the PI-RES parameters is also discussed in the paper.

Moreover, the LTPMSM's windings present a non-repetitive mutual coupling among the three phases due to the end effects [10-11]. This phase unbalance has a strong impact on the high-frequency motor model and makes the position tracking unstable without the adoption of a proper compensation method via look up table. Experimental results obtained using a LTPMSM prototype are shown in this paper to prove the feasibility of the proposed approach.

## II. LINEAR MOTOR MODELING

The high frequency model of the LTPMSM can be derived in the hypothesis that the injection pulsation  $\omega_i$  is much higher than the motor speed  $\omega_i \gg \omega_r$ , and the back-EMF voltage has no components at injection frequency [8]. Coil resistance and iron losses can be neglected because impedance practically coincides with reactance at injection frequency in the considered motor [4]. Moreover resistance only modifies the phase angle between voltages and currents that has no effect on the proposed demodulation strategy.

As it will be pointed out in the next section, the dq magnetic model of the linear motor (1) shows a cross coupling inductance term  $L_{dq}$  due to the end-effects. For the same reason all the inductances in the model are a function of

the electrical motor position  $\theta$ :

$$\begin{bmatrix} \lambda_d \\ \lambda_q \end{bmatrix} = \begin{bmatrix} L_d(\theta) & L_{dq}(\theta) \\ L_{dq}(\theta) & L_q(\theta) \end{bmatrix} \begin{bmatrix} i_d \\ i_q \end{bmatrix} \quad (1)$$

The variation of the inductances with the motor position is reported in figure 1b.

As will be explained later, the proposed sensorless control scheme impresses zero q-axis voltage (flux) at injection frequency. The inverse of (1) has to be derived in order to analyze the d-q current components. By using the complex notation [12] and introducing the complex-conjugate flux  $\lambda_{dq}^* = \lambda_d - j\lambda_q$ , (1) can be rewritten as (2) where positive and negative sequence components are evidenced:

$$\mathbf{i}_{dq} = \left( \frac{L_d(\theta) + L_q(\theta)}{2\Delta} \right) \lambda_{dq} - \left( \frac{L_d(\theta) - L_q(\theta)}{2\Delta} + j \frac{L_{dq}(\theta)}{\Delta} \right) \lambda_{dq}^* \quad (2)$$

where  $\Delta = L_d(\theta)L_q(\theta) - L_{dq}^2(\theta)$  and  $\mathbf{i}_{dq} = i_d + ji_q$ . In the following the dependence of all the inductances from the motor position  $\theta$  will be implied for simplicity.

In the proposed sensorless technique, a high-frequency pulsating current signal is injected on the estimated d-axis. For this reason, the equation (2) is rewritten using the estimated dq reference frame, that leads the actual dq frame by  $\theta_{err} = \theta^{est} - \theta$  radians ( $\mathbf{x}_{dq} = \mathbf{x}_{dq}^{est} e^{j\theta_{err}}$ ), as defined in figure 2:

$$\mathbf{i}_{dq}^{est} = \left( \frac{L_d + L_q}{2\Delta} \right) \lambda_{dq}^{est} - \left( \frac{L_d - L_q}{2\Delta} + j \frac{L_{dq}}{\Delta} \right) \lambda_{dq}^{est*} e^{-j2\theta_{err}} \quad (3)$$

The d-axis current controller is a proportional integral plus a resonant term (PI-RES) to ensure the tracking of the injected signal, but the q-axis current controller is a standard PI instead. The feedback q-axis current is low-pass-filtered so to remove the component at injection frequency that is above the q-axis current control loop cutoff frequency. In this way it is ensured that the q-axis reference voltage has negligible component at injection frequency, as above mentioned. Consequently, the flux along the estimated q-axis is zero ( $\lambda_{dq}^{est} = \lambda_{dq}^{est*} = \lambda_d^{est}$ ) and equation (3) becomes:

$$\mathbf{i}_{dq}^{est} = \left[ \left( \frac{L_d + L_q}{2\Delta} - \frac{L_d - L_q}{2\Delta} \cos(2\theta_{err}) - \frac{L_{dq}}{\Delta} \sin(2\theta_{err}) \right) + j \left( \frac{L_d - L_q}{2\Delta} \sin(2\theta_{err}) - \frac{L_{dq}}{\Delta} \cos(2\theta_{err}) \right) \right] \lambda_d^{est} = \mathbf{R} \lambda_d^{est} \quad (4)$$

where  $\mathbf{R}$  is a complex operator whose argument  $\psi$  is expressed in (5).

$$\psi = \arctan \left[ \frac{(L_d - L_q) \sin(2\theta_{err}) - 2L_{dq} \cos(2\theta_{err})}{(L_d + L_q) - (L_d - L_q) \cos(2\theta_{err}) - 2L_{dq} \sin(2\theta_{err})} \right] \quad (5)$$

The angle  $\psi$  is the phase angle of the obtained high frequency flux with respect to the injected current vector. It must be noticed that  $\psi$  is function of both the position

estimation error and the motor electrical position (by means of the  $L_d$ ,  $L_q$  and  $L_{dq}$  terms). Figure 3a reports the angle  $\psi$  as function of the motor position for different estimation error values.

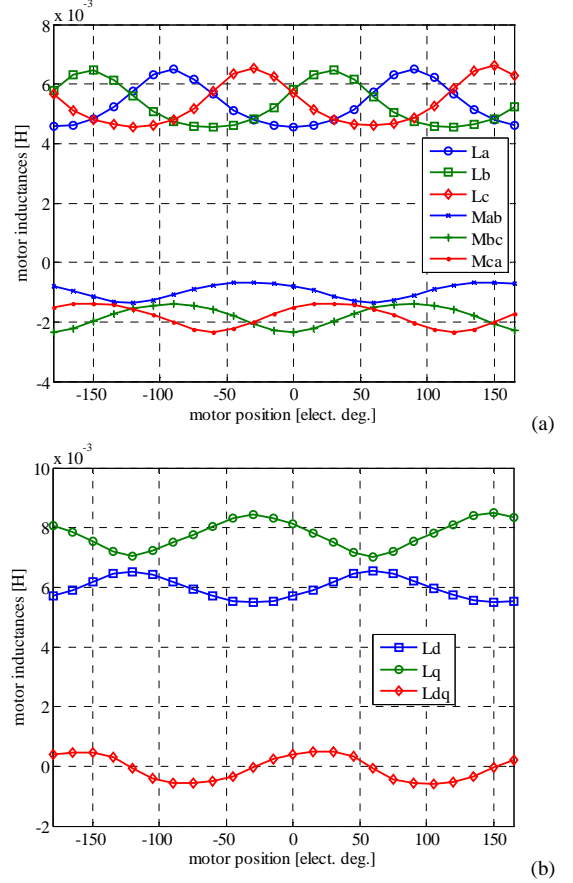


Fig. 1. Measured motor inductances at 1000 Hz in the abc (a) and dq (b) reference frame.

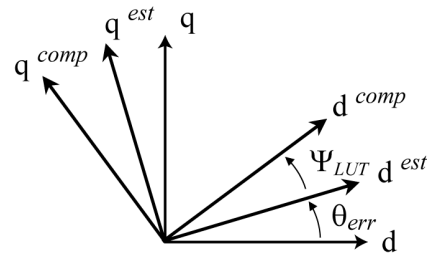


Fig. 2. Definition of the various reference frames needed for sensorless control: motor dq axes, estimated axes ( $d^{est}$ - $q^{est}$ ), axes for end effects compensation ( $d^{comp}$ - $q^{comp}$ ).

For a given estimation error  $\theta_{err}$ , the argument  $\psi$  varies with respect to the motor position and in particular the sign of  $\psi$  changes at different rotor positions. As already said, the dependence on  $\theta$  is due to the end effects of the tubular motor [10]. The red dashed curve in figure 3a demonstrates

that with no estimation error still the high-frequency current is still not aligned with estimated d-axis. In other words, having zero current along the estimated q-axis does not mean that the position is tracked correctly, as expected with rotating machines. A proper compensation method is then necessary. When the estimation error is zero the phase between flux and current becomes:

$$\psi_{LUT} = \arctan \left[ \frac{-L_{dq}}{L_q} \right] \quad (6)$$

The angle  $\psi_{LUT}$  is the red dashed line in figure 3a. It is convenient to introduce a compensated dq reference frame shifted from the estimated dq frame by  $\psi_{LUT} = \theta^{comp} - \theta^{est}$  radians ( $\mathbf{x}_{dq}^{comp} = \mathbf{x}_{dq}^{est} e^{-j\psi_{LUT}}$ ) as also defined in figure 2:

$$\mathbf{i}_{dq}^{comp} = \mathbf{i}_{dq}^{est} e^{-j\psi_{LUT}} = |R| \lambda_d^{est} e^{j(\psi - \psi_{LUT})} \quad (7)$$

The angle  $\psi - \psi_{LUT}$  is reported in figure 3b for the same values of  $\theta_{err}$  considered in figure 3a. In the compensated reference frame the sign of the phase angle between flux and current does not depend on motor position anymore, as clearly evidenced in figure 3b. Moreover the figure 3b shows that the q-axis current in the compensated reference frame at injection frequency will be null only if  $\theta_{err} = 0$ , because in the compensated reference frame, flux and current have real component only, when  $\theta_{err} = 0$ . The previous two sentences provide insight into the working principle of the proposed position observer described in section IV.

### III. SENSORLESS CONTROL SCHEME

When the PCV technique is adopted, the high-frequency pulsating current signal is only superimposed on the d-axis reference current because the injection on the q-axis would produce torque ripple. The d-axis is on the magnetic north pole of the rod. Since only the estimates of the rod position are available, the high-frequency pulsating current signal will be injected into the estimated d-axis. The d-axis current controller is a proportional integral plus a resonant term (PI-RES), needed to adequately follow the high-frequency current reference [13-14]. The PI-RES output is:

$$v_d^{est*}(s) = (i_d^{est*}(s) - i_d^{est}(s)) \left( k_p + \frac{k_i}{s} + k_{res} \frac{s}{s^2 + \omega_i^2} \right) \quad (8)$$

where  $\omega_i$  is the injecting pulsation,  $k_p$ ,  $k_i$  and  $k_{res}$  are the proportional, integral and resonant gain respectively. This controller structure is effective in regulating both the dc component and sinusoidal component simultaneously [13].

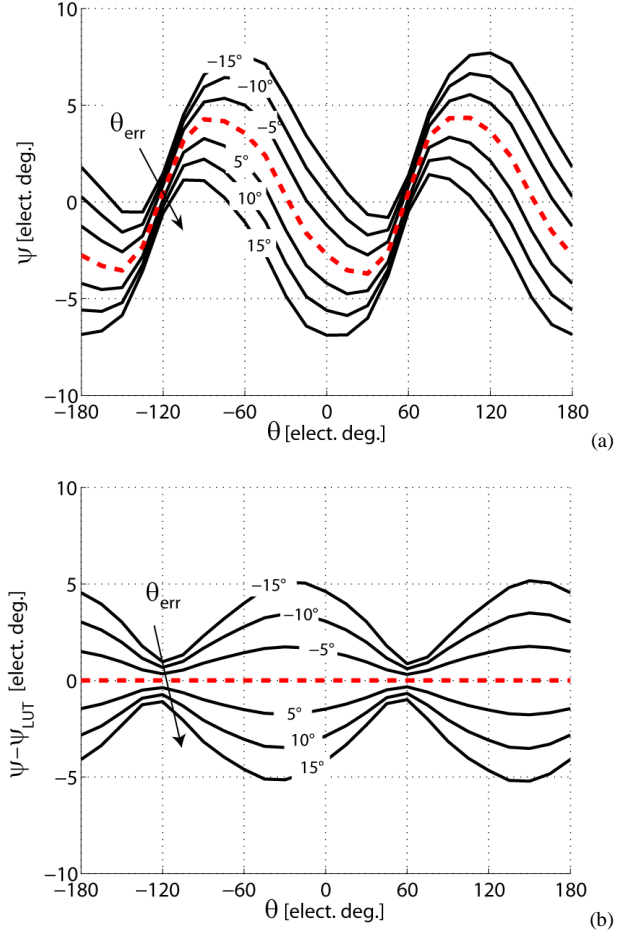


Fig. 3. Phase angle of the high-frequency current in the estimated (a) and in the compensated (b) dq reference frames for several values of the position estimation error between -15 and +15 electrical degrees.

As already mentioned, the q-axis current controller is a standard PI and the q-axis voltage reference at injection frequency can be neglected. The selection of the current controller gains will be discussed in the next section. Thanks to the adoption of a resonant controller, the actual  $i_d^{est}$  current will track precisely its reference  $i_d^{est*} = I \sin(\omega_i t)$ . The expression of  $i_d^{est}$  is then derived in equation (9) using (4):

$$i_d^{est} = |R| \lambda_d^{est} \cos(\psi) = I \sin(\omega_i t) \quad (9)$$

From (9), it is possible to obtain the relationship (10) between the flux amplitude and the injected current:

$$\lambda_d^{est} = \frac{I \sin(\omega_i t)}{|R| \cos(\psi)} \quad (10)$$

The current components in the compensated reference frame can be easily derived substituting the equation (10) in the (8), as shown below:

$$\begin{aligned} i_d^{comp} &= \frac{I \sin(\omega_i t)}{\cos(\psi)} \cos(\psi - \psi_{LUT}) \\ i_q^{comp} &= \frac{I \sin(\omega_i t)}{\cos(\psi)} \sin(\psi - \psi_{LUT}) \end{aligned} \quad (11)$$

The product of the current components (11) is given in (12) and is obtained applying Werner's formula:

$$i_d^{comp} i_q^{comp} = \frac{I^2}{2 \cos^2(\psi)} [1 - \cos^2(\omega_i t)] \sin(2(\psi - \psi_{LUT})) \quad (12)$$

A low pass filter can be used to remove the  $\omega_l$  component from (12):

$$LPF\{i_d^{comp}i_q^{comp}\} = \frac{I^2}{2\cos^2(\psi)} \sin(2(\psi - \psi_{LUT})) \quad (13)$$

Even if the term  $\cos^2(\psi)$  depends on the estimation error figure 3a shows that the angle  $\psi$  has relatively small values and, as a consequence, the coefficient  $I^2/2\cos^2(\psi)$  is almost constant. As demonstrated in figure 3b, the angle  $\psi - \psi_{LUT}$  is zero only when the estimation error is zero, thus (13) is the error function that will be used here for tracking the rotor position by means of a I-type regulator. It is important to underline again that the high-frequency current is injected along the estimated d-axis while the current demodulation is performed in the compensated dq reference frame in order to compensate the end-effects of the tubular motor.

The position can be obtained with an integrator that forces (13) to zero. In most the related literature the quantity to be minimized is the input of a PI regulator the output of which is the estimated motor speed and a further integrator is needed to obtain position [2-5]. The modified approach here introduced estimates the position by integration of  $LPF\{i_d^{comp}i_q^{comp}\}$  multiplied by the RMS value of  $v_d^{est*}$  and, successively, by integral gain (see figure 4). The RMS value is calculated using the last 16 samples, that correspond to one period of the 1 kHz injected voltage. In this way the number of parameters to be tuned is reduced so to simplify the commissioning of the position observer. Moreover it is exploited the condition that  $v_d^{est*}$  reaches its smaller amplitude when the estimation error is zero ( $L_q > L_d$  in the considered prototype). Multiplying by the RMS value of  $v_d^{est*}$  permits to increase the gain of the estimation loop when the estimation error increases, thus improving the observer performances during transients.

When a high-frequency voltage reference is added, the high-frequency current is distorted due to inverter non-idealities and a number of frequency components that could lie in the audible range. Moreover, the resistance variations introduce an uncertainty on the actual injected current amplitude. The PI-RES controller ensures sinusoidal current with constant

amplitude at injection frequency. The influence of inverter non-idealities (dead-time) on position estimate is greatly reduced with a small extra effort of tuning and computational cost. Although a PI-RES controller is required for the d-axis current, the q-axis controller can be a standard PI with no special requirements on its bandwidth. This simplifies the commissioning of the proposed scheme with respect to other approaches based on current injection.

A look-up table (LUT) stores the values of the angle  $\psi_{LUT}$ , given by equation (6), that are added to the estimated motor position  $\theta^{est}$  to obtain the position of the compensated dq reference frame used to implement the current demodulation algorithm. The estimated position is used for the coordinate transformation of the vector current control and for the injection of the high-frequency current signal. The LUT values were obtained using equation (6) together with the measured inductances. It can be also derived directly during the experiments. As a matter of fact the compensating LUT was also obtained experimentally changing the compensation angle until the estimation error became negligible during sensorless position control operations. The operation was repeated 56 times in different motor position covering 360 electrical degrees. The two LUTs are reported in figure 5 and agree quite well. They have a peak value of about 4 electrical degrees and do not depend on motor load. The motor under test has a very limited iron quantity on the rod that does not saturate for any current value and a back armature iron that is already saturated by the magnets at no load. Thus the saturation level is not affected by the armature current in the operating current range. It must be underlined that the considered motor is slotless. With slotted motors the core saturation (teeth, yoke and rod iron) can reduce the saliency and the signal to noise ratio of the tracking method, but this is a common issue of all saliency tracking methods.

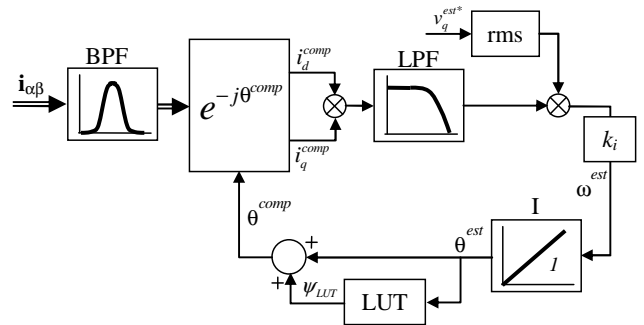


Fig. 4. Block diagram of the proposed position observer.

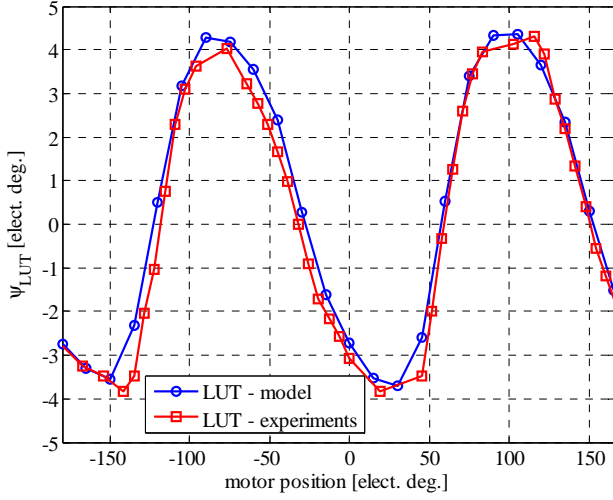


Fig. 5. Compensating LUT obtained using the mathematical model (blue circle) and directly measured under sensorless control (red square).



Fig. 6. LTPMSM prototype used for the tests.

#### IV. EXPERIMENTAL IDENTIFICATION OF THE LTPMM

The motor self and mutual phase inductances at injection frequency have been measured by means of a dedicated test bench. Each phase, in turn, was supplied with a 1000 Hz voltage with constant amplitude using a Chroma 61703 power supply. The current of the supplied motor phase and the voltages of the two non supplied phases were measured at different positions of the motor rod using oscilloscope probes. The test has been repeated three times for evaluating the self and mutual inductances of all the motor phases. The measured inductances are reported in figure 1a as function of motor position. The  $a$ - $b$  mutual term  $M_{ab}$  has a lower average value than the other two mutual terms. Phases  $a$  and  $b$  both have an end coil at the two opposite motor ends, while phase  $c$  does not. This justifies the reduced  $a$ - $b$  coupling that is lower than the  $a$ - $c$  and  $b$ - $c$  coupling as reported in figure 1a. The dq magnetic model introduced in equation (1) and figure

1b has been derived from the experimental phase inductances of figure 1a.

#### V. EXPERIMENTAL RESULTS

All the experimental investigations presented in this paper were performed using a dSPACE 1103 microcontroller board based on a Motorola Power PC microprocessor. Both motor and inverter are prototypes under development. Figure 6 shows the experimental test bench. The inverter switching frequency and the sample frequency of the control algorithm were set equal to 16 kHz, the inverter dead time is equal to 0.8  $\mu$ s. The rated LTPMSM parameters are as follows: current 2 A,  $R_s = 9 \Omega$ , polar pitch 56 mm ( $2\pi$  electrical radians), force constant 20 N/A, DC bus voltage 72 V.

The PI-RES controller was tuned considering that the resonant gain  $k_{res}$  has reduced influence on the step response of the system and the integral gain  $k_i$  has almost no effect on the response to a change of the high-frequency reference signal. It is worth to underline that the d-axis PI-RES controller usually works with d-axis current reference equal to zero in LTPMSM drives. The d-axis current reference is equal to zero to guarantee maximum torque per ampere ratio and the injected current has constant frequency  $f_i = 1000$  Hz and amplitude  $I = 0.5$  A. As a consequence, the quality of the transient response of the PI-RES controller is not crucial in the considered application. The d-axis current control loop has to be fast enough to guarantee robustness during torque transients (due to the coupling with the q-axis dynamics).

The procedure followed to select the PI-RES controller gains is divided into three steps. At first the time constant  $k_p/k_i$  is selected. The ratio  $k_p/k_i$  can lead to underdamped or overdamped step responses, as evidenced in figure 7. Then the proportional gain  $k_p$  is selected by looking at the system response after the application of a sinusoidal reference (see figure 8). Lower  $k_p$  values give more oscillations and longer transients. In the last step the resonant gain  $k_{res}$  is increased until the desired settling time after the application of a sinusoidal reference is reached. Figure 9 confirms that the gain  $k_{res}$  has no influence on the overshoot amplitude. The final gains used for position control test are  $k_p = 20$ ,  $k_i = 20000$ , and  $k_{res} = 10000$ . These numeric values, together with the sensitivity analysis presented in figures 7, 8 and 9 suggest that no fine tuning was necessary to obtain reasonable performances. The  $i_q$  PI controller gains were selected using the same  $k_p/k_i$  time constant. The proportional gain choice has to trade off between a higher cut-off frequency and the limitation of current ripple and acoustic noise. Proportional and integral gains were chosen equal to 10 and 10000 respectively. The closed loop Bode magnitude diagram measured under sensorless force control and reported in figure 10 evidences that the -3dB cutoff frequency of the  $i_q$  current control loop equals 560 Hz.

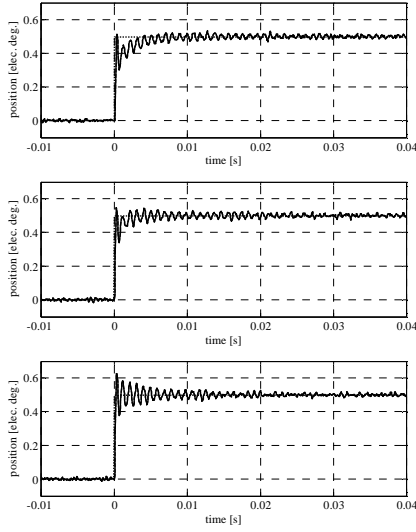


Fig. 7:  $i_d$  step response using  $k_p/k_i$  time constant equal to 2 ms (left), 1 ms (center), and 0.5 ms (right).

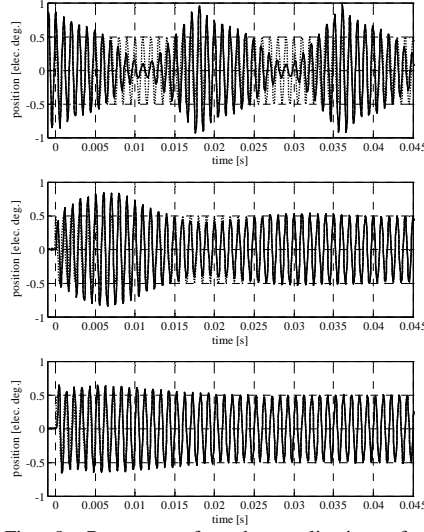


Fig. 8: Response after the application of a sinusoidal reference obtained using  $k_p=10$  (left),  $k_p=20$  (center), and  $k_p=30$  (right)

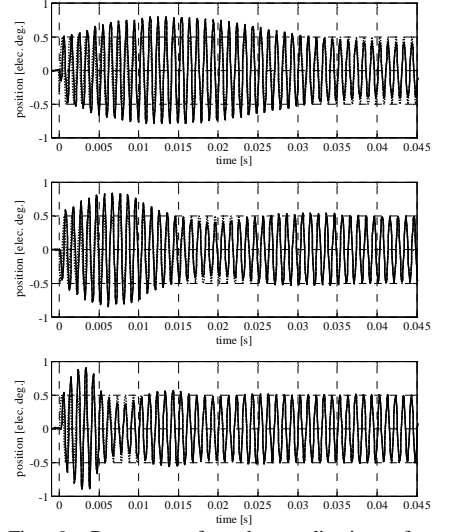


Fig. 9: Response after the application of a sinusoidal reference obtained using  $k_{res}=5000$  (left),  $k_{res}=10000$  (center), and  $k_{res}=20000$  (right)

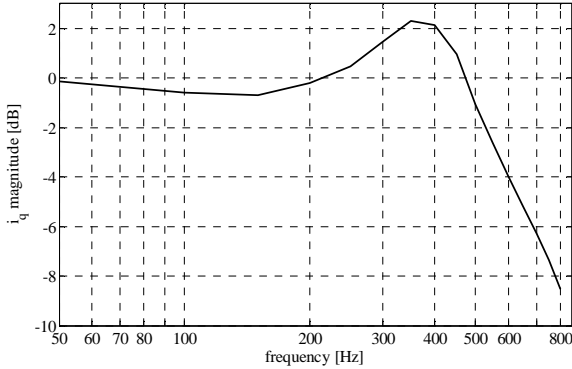


Fig. 10: Bode magnitude diagram for the  $i_q$  current control loop. The measured bandwidth under sensorless force control is equal to 560 Hz and comparable to the value reachable in sensed control.

Figure 11 reports the position response, the position estimation and tracking errors, and the  $i_q$  current response measured during a test in which a 20 N constant load was applied to the motor. The position reference was a minimum-time trajectory for a 28 mm (that corresponds to  $\pi$  radians) movement. The maximum acceleration was set equal to  $10 \text{ m/s}^2$  and the maximum speed equal to 200 mm/s (that corresponds to about 22.4 electrical radians per second). The maximum steady state estimation error is below half millimeter (3 electrical degrees) and slightly depends on both the applied load force and the absolute position. It is important to underline that the estimation error causes a reduction of the torque/ampere ratio. The transient error could be reduced by lowering the maximum speed of the position trajectory. The test shown in figure 11 has been repeated in no-load conditions and the obtained position estimation and tracking errors have been reported in figure

12. The similarity of the errors shown in figures 11b and 12 demonstrates that the performances are weakly related to the load, even when a LUT with constant parameters is adopted.

As term of comparison, table I reports the value of the integral absolute error (IAE) measured during the position trajectory of figure 11 using the proposed current injection (CI) scheme and a voltage injection (VI) scheme [3] to estimate the motor position. Both position and  $i_q$  current controller gains were set equal to those utilized in the test shown in figure 11. The amplitude of the injected voltage was selected so to obtain a high-frequency current equal to that utilized in the proposed current injection scheme.

The proposed current injection scheme reduces transient and steady-state estimation errors. The position tracking error is comparable because the regulator parameters are identical.

Finally, the effect of inverter dead time was investigated on both CI and VI schemes. The test shown in figure 11 was repeated several times increasing the dead time and leaving unaffected all the other control system parameters. While the VI scheme has stable behavior with dead time below  $2 \mu\text{s}$ , it was possible to run the CI scheme obtaining reasonable performances using dead time values up to  $4.8 \mu\text{s}$ . The power spectrum of the  $i_d$  current shown in figure 13 reveals a reduced leakage of the component at injection frequency using CI scheme. The reduced sensitivity to dead time increase can be considered an advantage of the proposed CI scheme over the standard VI one. The advantage is due to both the presence of the PI-PRES controller and the choice of estimating the rod position using the measured high-frequency q-axis current in place of the high-frequency q-axis voltage as proposed in previous CI schemes.



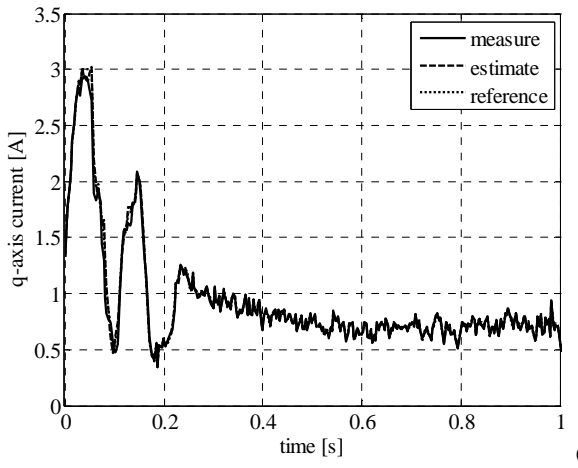
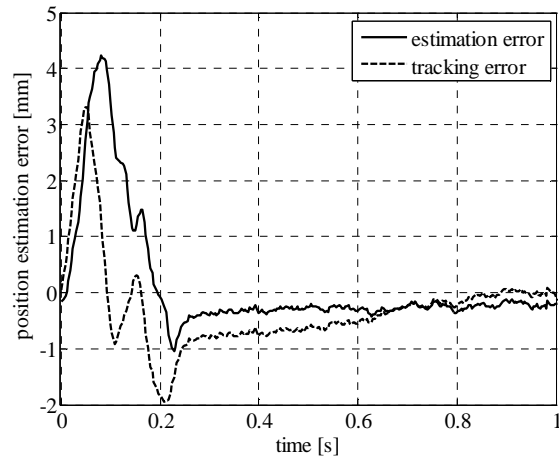
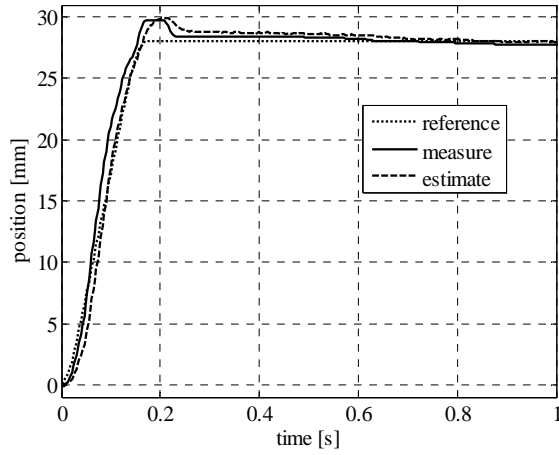


Fig. 11. Sensorless position control under 20 N constant load: position response (a), position estimation and tracking errors (b) and  $i_q$  current response (c).

TABLE I  
COMPARISON OF IAE AND PEAK ERROR VALUES OBTAINED USING CURRENT AND VOLTAGE INJECTION SCHEMES.

		Current Injection		Voltage Injection	
		No-load	Load	No-Load	Load
Estimation error	IAE [mm s]	1.18	1.23	1.27	1.52
	Peak [mm]	4.4	4.2	6.2	7.0
Tracking error	IAE [mm s]	0.76	1.18	1.04	1.54
	Peak [mm]	1.6	3.3	2.3	2.5

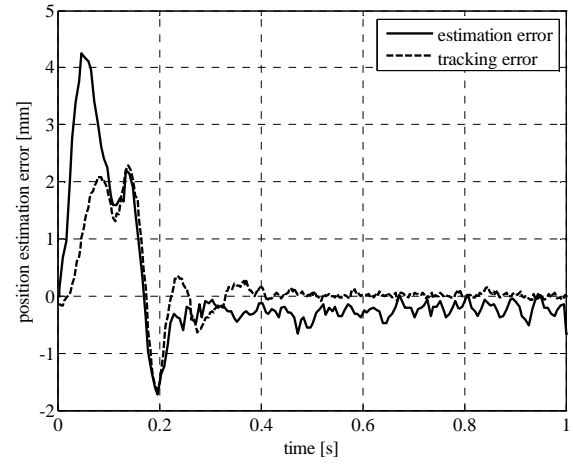


Fig. 12. Position estimation and tracking errors under no load test.

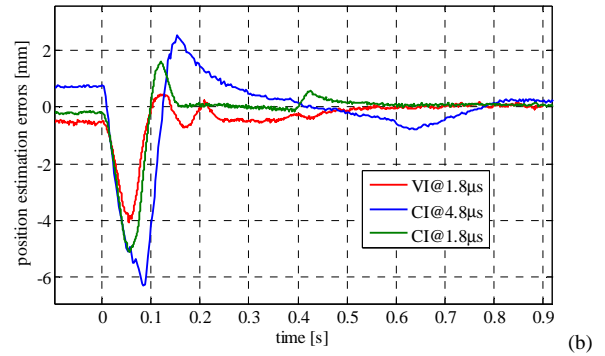
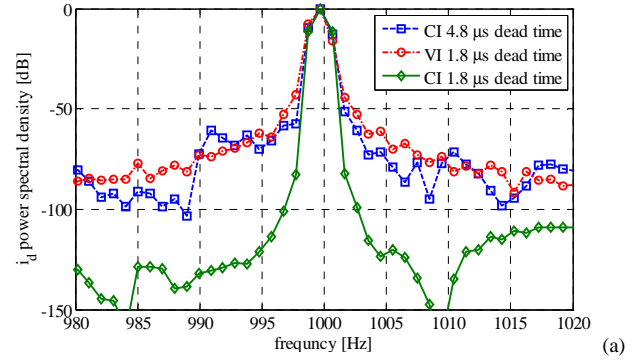


Fig. 13. Power spectral density of  $i_d$  current (a) and position estimation errors (b) obtained using voltage injection (VI) and current injection (CI) with different dead time values.



## VI. CONCLUSION

This paper presents a new position estimation scheme applied to linear low-saliency permanent magnet motors. The scheme is based on the injection of a pulsating high-frequency current along the d-axis and on the analysis of the q-axis motor current at the same frequency. It is simpler than existing current injection schemes because only requires the d-axis current controller able to track the injected current. With respect to voltage and current injection schemes proposed in the literature, the proposed position observer allows to reduce influence of the inverter non idealities. A position sensorless control scheme has been implemented using a LTPMM to verify the feasibility of the control scheme.

## REFERENCES

- [1] J. Holtz, "Sensorless Control of Induction Machines—With or Without Signal Injection?", *IEEE Transactions on Industrial Electronics*, Volume 53, Issue 1, Feb. 2006, pp. 7 – 30.
- [2] M. Linke, R. Kennel, and J. Holtz, "Sensorless speed and position control of synchronous machines using alternating carrier injection", *Proc. IEMDC 2003, IEEE Electric Machines and Drivers Conference*, Madison, WI, Jun. 2–4, 2003, pp. 1211 – 1217.
- [3] J. H. Jang, J. I. Ha, M. Ohto, K. Ide, and S. K. Sul, "Analysis of permanent magnet machine for sensorless control based on high frequency signal injection", *IEEE Trans. on Ind. Applications*, Vol. 40, n 6, Nov.-Dec. 2004.
- [4] J. Holtz, "Acquisition of Position Error and Magnet Polarity for Sensorless Control of PM Synchronous Machines", *IEEE Transactions on Industry Applications*, Vol. 44, n. 4, July-Aug. 2008 Page(s):1172 – 1180.
- [5] J. I. Ha; S. J. Kang, and S. K. Sul, "Position-controlled synchronous reluctance motor without rotational transducer" *IEEE Trans. on Ind. Applications*, Vol. 35, Issue 6, Nov.-Dec. 1999 pp.1393 – 1398.
- [6] S. J. Kang; J. M. Kim, and S. K. Sul, "Position sensorless control of synchronous reluctance motor using high frequency current injection" *IEEE Trans. on Energy Conv.*, Vol. 14, n. 4, Dec. 1999, pp. 1271 – 1275.
- [7] L. A. S Ribeiro, M. W. Degner, F. Briz, and R. D. Lorenz, "Comparison of carrier signal voltage and current injection for the estimation of flux angle or rotor position", *The 1998 IEEE 33rd IAS Annual Meeting*, 1998, Vol. 1, pp. 452 – 459.
- [8] D. Raca, P. Garcia, D. Reigosa, F. Briz, and R. D. Lorenz, "A comparative analysis of pulsating vs. rotating vector carrier signal injection-based sensorless control", *Proc. APEC 2008, IEEE Applied Power Electronics Conference and Exposition*, Feb. 24 – 28, Page(s): 879 – 885.
- [9] D. Raca, P. Garcia, D. Reigosa, F. Briz and R. D. Lorenz, "Carrier Signal Selection for Sensorless Control of PM Synchronous Machines at Zero and Very Low Speeds", *Proc. IEEE IAS Annual Meeting*, Phoenix, Arizona, 5-9 Oct. 2008, Edmonton, Canada.
- [10] O. Danielsson, and M. Leijon, "Flux Distribution in Linear Permanent-Magnet Synchronous Machines Including Longitudinal End Effects", *IEEE Transactions on Magnetics*, Vol. 43, Issue 7, July 2007 Page(s):3197 – 3201.
- [11] H. Polinder, J. G. Sloopweg, M. J. Hoeijmakers, and J. C. Compter, "Modeling of a linear PM Machine including magnetic saturation and end effects: maximum force to current ratio", *IEEE Transactions on Industry Applications*, Vol. 39, Issue 6, Nov.-Dec. 2003 Page(s):1681 – 1688.
- [12] P. Guglielmi, M. Pastorelli, and A. Vagati, "Cross saturation effects in IPM motors and related impact on zero-speed sensorless control", *IEEE Trans. on Industry Applications*, Vol. 42, Issue 6, Nov-Dec. 2006 Page(s):1516 – 1522.
- [13] M. Liserre, R. Teodorescu, and F. Blaabjerg, "Multiple harmonics control for three-phase grid converter systems with the use of PI-RES current controller in a rotating frame", *IEEE Trans. on Power Elect.*, Vol.21, n. 3, May 2006, pp 836 – 841.
- [14] D. N. Zmood, D. G. Holmes, and G. H. Bode, "Frequency-domain analysis of three-phase linear current regulators", *IEEE Trans. on Ind. Applications*, Volume 37, Issue 2, March-April 2001, pp 601 – 610.